Applied Catalysis B: Environmental 113–114 (2012) 296–307

Contents lists available at SciVerse ScienceDirect

Applied Catalysis B: Environmental

journal homepage: www.elsevier.com/locate/apcatb

Ni-based sol–gel catalysts as promising systems for crude bio-oil upgrading: Guaiacol hydrodeoxygenation study

M.V. Bykova*, D.Yu. Ermakov, V.V. Kaichev, O.A. Bulavchenko, A.A. Saraev, M.Yu. Lebedev, V.A. Yakovlev

Boreskov Institute of Catalysis SB RAS, Pr. Akad. Lavrentieva, 5, Novosibirsk 630090, Russia

ARTICLE INFO

Article history:
Received 17 August 2011
Received in revised form
25 November 2011
Accepted 29 November 2011
Available online 7 December 2011

Keywords:
Guaiacol
Hydrodeoxygenation
Hydrogenation
Ni-based catalysts
Bio-oil
Biofuel

ABSTRACT

Catalytic hydrotreatment or hydrodeoxygenation (HDO) has been researched extensively with the crude bio-oil and its model compounds over conventional sulfided Ni(Mo), Co(Mo) catalysts and supported noble metal catalysts. These types of catalysts showed themselves unsuitable for the target HDO process, which resulted in an urgent need to search for a new catalytic system meeting such requirements as low cost, stability against coke formation and leaching of active components due to adverse effect of the acidic medium (bio-oil). In the present work a series of Ni-based catalysts with different stabilizing components has been tested in the hydrodeoxygenation (HDO) of guaiacol (2-methoxyphenol), bio-oil model compound. The process has been carried out in an autoclave at 320 °C and 17 MPa H_2. The main products were cyclohexane, 1-methylcyclohexane-1,2-diol, and cyclohexanone. The reaction scheme of guaiacol conversion explaining the formation of main products has been suggested. The catalyst activity was found to rise with an increase in the active component loading and depend on the catalyst preparation method. The most active catalysts in HDO of guaiacol were Ni-based catalysts prepared by a sol–gel method and stabilized with SiO_2 and ZrO_2. According to TPR, XRD, XPS, and HRTEM, the high activity of these catalysts correlates with the high nickel loading and the high specific area of active component provided by the formation of nickel oxide–silicate species. The effect of temperature on the product distribution and catalyst activity in the target process (HDO) has been investigated as well. The catalysts were shown to be very promising systems for the production of hydrocarbon fuels by the catalytic upgrading of bio-oil.

1. Introduction

For the recent decades processes of biomass conversion into hydrocarbon fuels has been attracting much attention due to decreasing of crude-oil reserves, enhanced demand for fuels worldwide and increased climate concerns about the use of fossil-based energy carriers. In contrast to fossil fuel reserves, biomass is indicated as an abundant, sustainable and carbon-neutral renewable energy resource for the production of biofuels and valuable chemicals. Fast pyrolysis technology is commonly used for the biomass conversion into liquid products, referred to as bio-oil [1]. Usually bio-oil contains water (15–30%), a heavy lignin fraction (20%), and different organic compounds (50–65%) such as aldehydes, ketones, organic acids, furans, methoxyphenols, sugar derivatives, *etc.* [2,3]. The bio-oil composition depends on the type of feedstock (biomass) and the pyrolysis conditions. The direct use of bio-oil without any additional treatments is complicated due to a high viscosity of bio-oil, its thermal and chemical instability as well as its tendency to the polymerization during storage and transportation. These disadvantages are due to the high content of oxygen in the liquid products of the fast pyrolysis [4].

Nowadays, the fast pyrolysis products are usually upgraded via their hydrotreatment. The key reaction of this process is the hydrogenolysis of C—O bonds (hydrodeoxygenation) of oxygen-containing compounds with the formation of water [5,6]. Hydrodeoxygenation (HDO) of crude bio-oil and its model compounds has been investigated extensively [7–12]. Guaiacol is of great interest as such a model compound of bio-oil, because the presence of two oxygen-containing functional groups in it (phenolic (—OH) and methoxy ($—OCH_3$) groups) provides its ability to the repolymerization, which is the inherent characteristic of bio-oil under thermal treatments [4,13]. As a result, a number of papers were devoted to the investigation of guaiacol hydrodeoxygenation [11,14–20], in which a few schemes of guaiacol conversion, including the formation of such products as catechol, phenol, benzene, cyclohexanone, cyclohexanol, cyclohexane, and methyl-substituted phenols, have been proposed. It was shown that the phenolic $C_{aromatic}$—O bond is stronger than the O—CH_3 bond of the

* Corresponding author. Tel.: +7 383 326 96 52; fax: +7 383 330 62 54.
E-mail address: bykova@catalysis.ru (M.V. Bykova).

0926-3373/$ – see front matter © 2011 Elsevier B.V. All rights reserved.
doi:10.1016/j.apcatb.2011.11.051

Table 1
Chemical composition and textural characteristics of the catalysts activated in hydrogen at 400 °C.

No.	Active component[a] (wt%)		Stabilizing component	A_{BET} (m^2/g)	V_{Σ} (cm^3/g)	$V_{\mu pore}$ (cm^3/g)	⟨d⟩ (Å)
	Ni	Cu					
1	14.1	5.7	δ-Al_2O_3	109	0.31	–	112
2	30.3	10.4	CeO_2 (21.5%)–ZrO_2 (27.0%)	82	0.15	–	71
3	36.5	2.3	SiO_2 (12.6%)–ZrO_2 (37.2%)–La_2O_3 (0.9%)	66	0.05	0.002	30
4	55.4	–	SiO_2	216	0.17	0.05	20
5	57.9	7.0	SiO_2	142	0.11	0.03	24

[a] For the initial oxide form of the active components.

guaiacol methoxy group, and therefore its cleavage requires more severe conditions (high temperature and high pressure) [21]. At the same time, such conditions are favorable for the guaiacol polymerization leading to the tar formation as a precursor of a solid coke-like product [14].

Catalytic hydrotreatment of bio-oil and its model compounds was studied extensively over conventional sulfided Ni(Mo) and Co(Mo) hydrotreatment catalysts supported on γ-alumina [11,16,22]. Supported catalysts with noble metals (Pt, Pd, Ru, Rh) as active components were also studied, although to a lesser extent [9,14,23]. Different supports such as SiO_2-Al_2O_3 [23], CeO_2-ZrO_2 [10], MgO [8], ZrO_2 [9,14,16], activated carbon [12], SiO_2 [15,24], *etc*. were used with both types of active components. It was shown that the noble-metal catalysts supported on ZrO_2 and SiO_2 had a higher catalytic activity in HDO of bio-oil and its model compounds than the conventional sulfided NiMo/γ-Al_2O_3 and CoMo/γ-Al_2O_3 catalysts [14,24]. However, the high cost of noble-metal catalysts prevents their wide practical application. On the other hand, sulfided catalysts are quickly deactivated because of a low content of sulfur in an initial feedstock, leading to a sulfur removal from the catalysts followed by coke formation. Moreover, the final products are contaminated with sulfur [14]. Therefore, it is necessary to develop such noble-metal-free catalysts that would satisfy such requirements as a low cost, a non-sulfided nature, a high activity in the HDO process, a high stability against coke formation under reaction conditions, and ability for repeated regeneration.

Very recently, non-sulfided Co-Mo-B and Ni-Mo-B amorphous catalysts prepared by chemical reduction of corresponding metal salts with sodium borohydride have been tested in HDO of bio-oil model compounds [7,25]. A number of transition metal (Ni, Fe, Mo, Co, W) phosphides supported on silica, which are considered as a prospective type of hydrotreatment catalysts [26], were also investigated in HDO of guaiacol by Zhao et al. [15]. The positive effect of P and B additives on the catalyst activity in the target reaction was observed in both cases. However, the catalysts possessed an insufficient stability due to the loss of B and P during the reaction which led to the agglomeration of active component particles.

It is well known that nickel is much less expensive than noble metals, besides it is highly active in the hydrogenation reactions [27]. Copper addition facilitates reduction of nickel oxide at lower temperature [28] and decreases the coke formation rate [29]. Correspondingly, Ni-based catalysts also were studied in the hydrodeoxygenation of bio-oil model compounds. For example, Yakovlev et al. [10] showed that NiCu-catalysts prepared by the impregnation of δ-Al_2O_3, ZrO_2, CeO_2 supports with solutions of corresponding metal salts have a moderate activity in the hydrodeoxygenation of oxygen-containing compounds. Based on catalyst testing, authors made a conclusion that these catalytic systems are of interest for the bio-oil upgrading. Nevertheless, to prepare catalysts with the high loading of active component and, therefore, to increase the catalytic activity, another preparation method (the co-precipitation of active component precursors) can be used. Besides, the agglomeration of active component particles has to be taken into account in the case of high-loaded catalysts. To prevent this undesirable effect, different stabilizing components have to be used.

The aim of the present work was the investigation of Ni-based catalysts with high metal loading and different active-phase stabilizing components, such as δ-Al_2O_3, SiO_2, SiO_2-ZrO_2, CeO_2-ZrO_2, in HDO of guaiacol. Some catalysts were promoted with copper. In addition, the effect of temperature on the product distribution and catalyst activity in the target process (HDO) was studied. The catalysts with the highest activity in HDO of guaiacol were characterized by TPR, XRD, XPS, and HRTEM techniques to establish the correlation between the catalyst structure and activity.

2. Experimental

2.1. Catalyst characterization

The catalysts were prepared by the following methods. Samples No. 1 and No. 2 (Table 1) were prepared by the wet impregnation with solutions of corresponding metal salts. Sample No. 1 was supported on a commercial support γ-Al_2O_3 (Sasol Company) calcined at 1000 °C while sample No. 2 was supported on a mixed oxide CeO_2-ZrO_2 prepared by the co-precipitation [30]. Samples No. 3–5 were prepared by the sol–gel method described elsewhere [31]. After preparation by the method [31] sample No. 3 was additionally impregnated by $ZrO(NO_3)_2$ and $La(NO_3)_3$ salt solutions to improve catalyst mechanical and thermal stability. Then the catalyst was dried at 150 °C and calcined at 400 °C. The notation system used in this work can be exemplified by catalyst No. 3: Ni36.5Cu2.3/ZrO_2-SiO_2-La_2O_3. In front of the slash, the catalyst active components (Ni and Cu) are specified; numbers correspond to the mass percentages of the elements in the initial oxide form of the catalyst. The type of stabilizing component is given behind the slash. The results of elemental analysis for the fresh catalysts are presented in Table 1. Textural characteristics of the catalysts after activation in hydrogen at 400 °C are presented in Table 1.

2.2. Catalytic activity tests

Catalysts were tested in HDO of guaiacol on a high-pressure set up (Autoclave Engineers, USA) in a sealed 300 mL stainless steel batch reactor (EZE Seal type). The reactor was equipped with a magnetic stirrer, a thermocouple, a pressure sensor, and a system for controlling stirring rate, temperature and pressure. Before the reaction, the catalysts (1 g, 0.05–0.1 mm fraction) were activated directly in the reactor by the reduction in a flow of 100% H_2 (100 mL/min) for 1 h at 400 °C and 0.1 MPa. After the activation, 30 mL of guaiacol (Acros Organics, 99%) was placed into the reactor at 0.1 MPa and 25 °C without access of air to prevent the catalyst oxidation. After that, the reactor was pressurized to 11 MPa H_2 at room temperature and then sealed. The hydrogen-to-guaiacol molar ratio was kept the same in all experiments. Further, the reactor was heated by an oven until the preset temperature (320 °C), which led to a pressure increase up to 17 MPa. The reaction

duration was taken to coincide with the stirring time, which was equal to 1 h. The stirring rate was 2000 rpm. The reaction was accompanied with a gradual pressure decrease, which was not compensated by addition of hydrogen. After the reaction, the reactor was cooled to room temperature, and liquid and gaseous products were analyzed.

2.3. Product analysis and principal definitions

Qualitative analysis of the guaiacol HDO liquid products was carried out using a Varian Saturn 2000 GC/MS spectrometer equipped with an ion trap, and an HP 5 quartz capillary column (stationary phase: 5% phenyl–95% dimethylpolysiloxane, column length of 30 m, inner diameter of 0.25 mm). Quantitative analysis of the liquid products was performed on a Chromos GCh 1000 chromatograph equipped with a Zebron ZB-35HT INFERNO capillary column (stationary phase: 35% phenyl–65% dimethylpolysiloxane, 30 m × 0.32 mm × 0.25 μm). The gas phase (H_2, CO, CO_2, CH_4) was analyzed on a Chromos GCh 1000 chromatograph equipped with two columns packed with silochrome or activated carbon (3 m × 2 mm i.d.) and with thermal conductivity and flame ionization detectors, respectively.

The catalyst activity was estimated according to guaiacol conversion X_{GUA}(%) and deoxygenation degree HDO (%), which were calculated as follows:

$$X_{GUA}(\%) = \frac{n^0_{GUA} - n^{final}_{GUA}}{n^0_{GUA}} \times 100 = X \times 100 \quad (1)$$

$$HDO(\%) = \frac{n^0_{GUA} \times X \times 2 - \sum_i n_i a_i}{n^0_{GUA} \times X \times 2} \times 100 = \left(1 - \frac{\sum_i n_i a_i}{n^0_{GUA} \times X \times 2}\right) \times 100 \quad (2)$$

where n^0_{GUA} is the initial amount of guaiacol (mol), n^{final}_{GUA} is the final amount of guaiacol (mol), n_i is the amount of i-product (mol) in the liquid phase (except for unreacted guaiacol), and a_i is the number of oxygen atoms in the molecule of i-product.

The product distribution was calculated as:

$$\varphi_i(\%) = \frac{n_i}{\sum_{i=j}^{k} n_i} \times 100 \quad (3)$$

where φ_i(%) is the fraction of i-product in the liquid phase, taking into account unreacted guaiacol.

Product selectivities and product yields were calculated according to Eqs. (4) and (5), respectively:

$$S_i(\%) = \frac{n_i}{A_i/A_{GUA} \times n^0_{GUA} \times X} \times 100 \quad (4)$$

$$W_i(\%) = \frac{n_i}{A_i/A_{GUA} \times n^0_{GUA}} \times 100 = S_i \times X \quad (5)$$

where A_i and A_{GUA} are stoichiometric coefficients in the reaction of guaiacol conversion into i-product.

2.4. Catalyst characterization

2.4.1. Texture characteristics

Texture characteristics of the catalysts were measured at the liquid nitrogen temperature using an ASAP-2400 automated volumetric adsorption analyzer (Micromeritics Instrument. Corp., USA). Before the analysis, the samples were calcined at 150 °C and pressure 0.13 Pa for 4 h. The analysis time was varied depending on the particular sample. The resulting adsorption isotherms were used to calculate the specific surface area A_{BET}, the total pore volume V_Σ (from ultimate adsorption at a relative pressure of $P/P_0 = 1$), the micropore volume V_μ, and the mean pore size.

2.4.2. Temperature-programmed reduction

The TPR studies were performed in a 10% H_2 + 90% Ar mixture at a flow rate of 30 mL/min. The catalyst sample weight was varied according to the metal content (m_{met} = 50 mg). The sample was placed into a U-shaped quartz reactor and was heated to 800 °C at a constant rate of 6 °C/min in the reductive medium. The outlet concentration of hydrogen was recorded using a thermal conductivity detector.

2.4.3. X-ray diffraction

XRD studies were performed on an ARL X'TRA powder diffractometer (Thermo, Switzerland) using the monochromatic Cu Kα radiation (λ = 0.1542 nm). X-ray diffraction patterns were recorded in a step scan mode in the 2θ range from 15° to 70° with the step of 0.05° using a counting time of 3 s per step. The mean size of the coherent-scattering domain (CSD) was determined based on the broadening of the reflections using the Selyakov–Scherrer equation. The *in situ* XRD study of the catalyst reduction was carried out on a D500 Siemens X-ray diffractometer (Germany) equipped with a home-made reactor chamber. The reduction was performed by heating the catalyst to 350 °C with the rate of 25 °C/min at 0.1 MPa H_2 and a flow rate of 30 mL/min. Heated samples were kept at the final temperature for 1 h. The XRD patterns were obtained *in situ* after cooling down to 25 °C.

2.4.4. X-ray photoelectron spectroscopy

X-ray photoelectron spectroscopy was applied for the chemical analysis of the catalyst surface. XPS studies were performed on a SPECS's machine (Germany) equipped with an X-ray source XR-50M with a twin Al/Ag anode, an ellipsoidal crystal X-ray monochromator FOCUS-500, and a hemispherical electron energy analyzer PHOIBOS-150. The photoelectron spectrometer was also equipped with a high-pressure cell with a volume of about 1 L, which enabled the heating of samples in gaseous mixtures at pressures up to 0.5 MPa. The XPS spectra were obtained using the monochromatic Al Kα radiation (h = 1486.74 eV) and a fixed analyzer pass energy of 20 eV under ultrahigh vacuum conditions. The binding energy scale was calibrated by the internal standard method using the $Ni2p_{3/2}$ peak at 852.7 eV from nickel in the metallic state. Relative element concentrations were determined from the integral intensities of XPS peaks using the cross-sections according to Scofield [32]. For detailed analysis the spectra were deconvoluted onto several peaks after the background subtraction by the Shirley method [33]. The deconvolution was performed using the CasaXPS software [34]. The line shapes were approximated by a convolution of Gaussian and Lorentz functions.

Two types of catalysts – in the initial oxide form and after the activation in hydrogen at 400 °C and 0.1 MPa followed by passivation with ethanol – were examined by XPS. Before the reduction, powder samples were pressed into thin self-supporting wafers with a diameter of 9 mm and a thickness of 1 mm. The catalysts activated in hydrogen were additionally reduced in the high-pressure cell of the XPS machine at a hydrogen pressure of 0.1 MPa at 400 °C for 1 h. Thereafter, the catalysts were cooled down to the room temperature, vacuumized and transferred to the analysis chamber without a contact with air.

2.4.5. High resolution transmission electron microscopy

HRTEM images were obtained on a JEM-2010 (JEOL, Japan) electron microscope with a lattice resolution of 0.14 nm and an accelerating voltage of 200 kV. The samples for the HRTEM study were prepared by the ultrasonic dispersing in ethanol and consequent deposition of the suspension upon a "holey" carbon film

Table 2
Guaiacol conversion, deoxygenation degree, and product distribution in HDO of guaiacol performed in the autoclave at 320 °C and initial hydrogen pressure of 17 MPa, reaction time - 1 h, $m_{GUA}:m_{cat}$ = 33:1.

Catalyst	Product distribution (liquid phase) (mol%)[a]				Balance of carbon			X_{GUA} (%)	HDO (%)
	Aliph. + benzene[b]	Aliph. – O[c]	Arom – O[d]	Condenses[e]	Liquid phase (mol%)	Gas phase (mol%)	Solid phase (mol%)/coke on the catalyst (wt%)		
Ni30.3Cu10.4/CeO_2-ZrO_2	1.6	92.5	0.4	0	92.5	7.4	0.1/2.3	94.2	33.3
Ni14.1Cu5.7/Al_2O_3	49.9	28.9	0.9	1.1	96.7	3.0	0.3/6.8	80.3	71.2
Ni57.9Cu7.0/SiO_2	72.7	7.1	3.0	4.2	90.1	9.8	0.1/2.3	87.1	91.5
Ni36.5Cu2.3/ZrO_2-SiO_2-La_2O_3	80.1	2.7	1.9	1.6	91.9	8.0	0.1/2.3	85.6	96.1
Ni55.4/SiO_2	90.9	1.4	2.1	3.1	89.3	10.0	0.7/15.8	97.5	97.3

[a] Molar fraction of products in the liquid phase, taking into account unreacted guaiacol.
[b] Aliphatics C_5–C_7 + benzene (total deoxygenation products).
[c] O-containing aliphatics C_5–C_7.
[d] O-containing aromatics (phenol, methoxybenzene, methoxy-methylphenol).
[e] Products of aromatic ring condensation.

supported on a copper grid. Local elemental analysis was performed with the EDX method on an energy-dispersive X-ray Phoenix spectrometer equipped with a Si(Li) detector with an energy resolution of 130 eV.

3. Results and discussion

3.1. Catalyst testing in HDO of guaiacol

As a matter of fact, a considerable number of guaiacol hydrodeoxygenation studies have been reported in the literature [11,14–20]. Guaiacol HDO was carried out in batch reactors [14,18,20] or in fixed bed reactors [11,17,19]. In most of these studies a guaiacol solution in different solvents (tetradecane, n-hexadecane, decalin, water) was used to simulate the pyrolysis oil [14,16,18,20] and several guaiacol conversion schemes were proposed [11,15–19]. These schemes include the formation of both aromatic products (benzene, toluene, phenol and substituted phenols) and aliphatic hydrocarbons (cyclohexane, cyclohexanol, cyclohexanone, *etc.*), as well as the formation of condensation products. Both parallel and consecutive routes of the formation of these products were considered. Overall, the guaiacol conversion pathways are mainly determined by the presence of phenolic and methoxy groups.

(1) *Reactions of CH_3O-group* are *demethylation* by the hydrogenolysis of the O—CH_3 bond of the methoxy group resulting in the formation of catechol and methane as the sub-product, or *demethoxylation* via the cleavage of the $C_{aromatic}$—OCH_3 bond with the formation of phenol and methanol [18,35].
(2) In the case of *phenolic OH-group*, the first conversion pathway is the hydrogenolysis of the $C_{aromatic}$—OH bond, while the second pathway involves the hydrogenation of the initial aromatic ring followed by the OH-group elimination [11,18].

In the present study a pure guaiacol was used as a feedstock without using any solvent in contrast to most of guaiacol studies reported in the literature. The guaiacol conversion and deoxygenation degree calculated based on the analysis of liquid and gaseous products are shown in Table 2. All these experiments were performed at least in duplicate and were well reproducible. The standard deviations of the values obtained were not more than 5%. According to the data presented in Table 2, Ni57.9Cu7.0/SiO_2, Ni55.4/SiO_2, and Ni36.5Cu2.3/ZrO_2-SiO_2-La_2O_3 are the most active catalysts in the target process. Although the guaiacol conversion was sufficiently high (80–97%) over all samples, these three catalysts provided the highest deoxygenation degree (92–97%). It can be easily noted that even though a pure guaiacol was used without addition of solvent in this study, all catalysts tested showed HDO activity and high guaiacol conversion.

The product distribution observed in HDO of guaiacol is shown in Table 2. The total deoxygenation products like C_5–C_7 aliphatic hydrocarbons and benzene were used to estimate the HDO effectiveness and the catalyst activity. To estimate the degree of aromatic ring hydrogenation, oxygen-containing aliphatic and aromatic products were divided into two separate groups. In the case of Ni30.3Cu10.4/CeO_2-ZrO_2, C_5–C_7 aliphatic hydrocarbons with oxygen-containing functional groups (cyclohexanol, cyclohexanone, 1-methylcyclohexane-1,2-diol, *etc.*) compose the largest fraction of guaiacol HDO products. In contrast, the catalysts Ni57.9Cu7.0/SiO_2, Ni36.5Cu2.3/ZrO_2-SiO_2-La_2O_3, and Ni55.4/SiO_2 led to the formation of mostly oxygen-free aliphatic hydrocarbons (mainly cyclohexane) in the liquid phase, which are the target products of total deoxygenation.

The mass balance was calculated with respect to the initial amount of carbon atoms in 30 mL of guaiacol (mol%). As shown in Table 2, the liquid product content was almost the same over all catalysts and was close to 90%, while the total fraction of gaseous and solid products did not exceed 11%. The only exception was Ni14.1Cu5.7/Al_2O_3, which showed relatively high coking degree on the one hand, and the low yield of methane on the other hand. The amount of gaseous products (mainly CH_4) increases with the nickel loading, which is in good agreement with the published data [10,36] on the hydrocarbon methanization over Ni-based catalysts. According to thermogravimetric analysis (TGA), the largest amount of coke was observed on the monometallic catalyst with the high nickel loading Ni55.4/SiO_2. On the contrary, the less amount of coke that was observed on Ni57.9Cu7.0/SiO_2 can be attributed to the presence of copper. The coke formation on Ni14.1Cu5.7/Al_2O_3, a catalyst with copper and with the low content of Ni, is likely due to the presence of acidic centers on the catalyst support.

Hence, taking into account the combination of such factors as the guaiacol conversion, the deoxygenation degree, the amount of undesired gaseous products, and the coking extent on the catalyst surface, Ni36.5Cu2.3/ZrO_2-SiO_2-La_2O_3 was chosen as the most promising catalyst for HDO of bio-oil and its model compounds.

Fig. 1 illustrates the percent (φ) of the main liquid-phase products (cyclohexane, benzene, 1-methylcyclohexane-1,2-diol, and cyclohexanone) obtained during the catalyst testing in HDO of guaiacol. The yields (W_i) of all guaiacol conversion products are presented in Table 3. The products of isomerization (dimethylcyclopropane, cyclopentane) and aromatic ring condensation (Fig. 2: bicyclohexyl, 2-cyclohexylphenol, cyclohexylbenzene, and 2-cyclohexylcyclohexanol) also were detected in the liquid phase.

As can be seen from Fig. 1, the reaction over Ni30.3Cu10.4/CeO_2-ZrO_2 resulted in the formation of a sufficient amount of

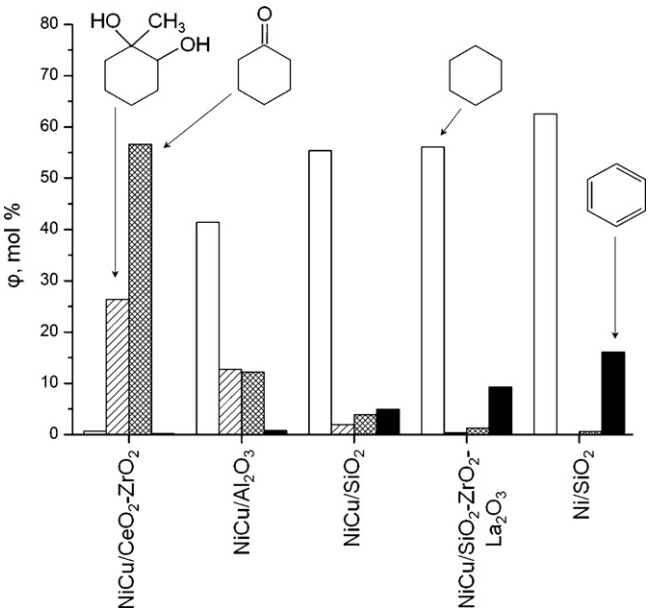

Fig. 1. Distribution of the main liquid products (φ, mol%) obtained in HDO of guaiacol over Ni-based catalysts in the autoclave at 320 °C, starting hydrogen pressure of 17 MPa, reaction time 1 h.

cyclohexanone (about 57 mol%), and 1-methylcyclohexane-1,2-diol (27 mol%). The maximal amounts of cyclohexane were formed over Ni57.9Cu7.0/SiO_2, Ni36.5Cu2.3/ZrO_2-SiO_2-La_2O_3, and Ni55.4/SiO_2.

Based on these data, the following main routes of guaiacol conversion over high-loaded Ni-based catalysts can be assumed:

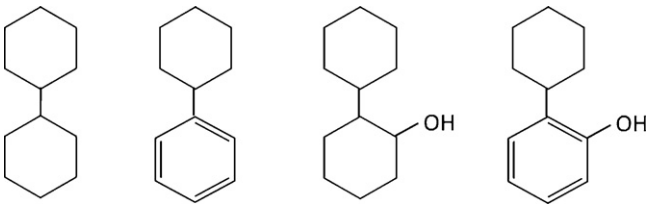

Fig. 2. Products of aromatic ring condensation identified by GC–MS.

(1) Methyl group migration to the aromatic ring with the formation of two hydroxyl groups and the following hydrogenation of the aromatic ring with the formation of 1-methylcyclohexane-1,2-diol.
(2) Guaiacol conversion to phenol via either the direct demethoxylation or the demethylation into catechol (1,2-benzenediol) with its subsequent partial hydrodeoxygenation; thereafter the hydrogenation of the phenol aromatic ring into cyclohexanol with its further transformation into cyclohexane. Cyclohexane can be also formed via guaiacol hydrodeoxygenation to benzene with its following hydrogenation.
(3) Guaiacol demethylation into catechol and its further hydrogenation to 1,2-cyclohexanediol; then dehydration of 1,2-cyclohexanediol into unstable cyclic enol with its transformation into cyclohexanone via the keto-enol tautomerism. Cyclohexanone can be also formed via partial hydrogenation of phenol into cyclohexenol with its following keto-enol isomerization.

In the case of Ni30.3Cu10.4/CeO_2-ZrO_2, the guaiacol conversion proceeds mainly through the 1st and 3rd routes. The 2nd route can be assumed to prevail in the case of Ni57.9Cu7.0/SiO_2, Ni36.5Cu2.3/ZrO_2-SiO_2-La_2O_3, and Ni55.4/SiO_2, because of the significant amount of benzene and the small amount of oxygen-containing aliphatic hydrocarbons observed over these catalysts. Hence, according to our results and data available from the literature, the following scheme of the guaiacol conversion over Ni-based catalysts can be suggested (Scheme 1).

Hereby, the catalytic conversion of guaiacol in the present work involved two major classes of reactions: hydrodeoxygenation and hydrogenation, as was earlier reported by other researches. It is to be noted that some guaiacol conversion schemes reported in the literature also included transalkylation reactions with the methyl group transfer into the aromatic ring [11,17,19]. These reactions were observed when using catalysts with acidic nature of the support, usually γ-alumina or silica–alumina. The use of such supports led to demethylation/methyl-substitution reactions after C(sp3)—O cleavage and the formation of the methyl-substituted aromatic products. In the present guaiacol HDO study a considerable amount of methyl substituted cyclohexandiol was formed. It is proposed that this could be due to methyl transfer reaction of guaiacol and further hydrogenation of methylcatechol. The same methyl

Table 3
Yields (W_i) % of products in HDO of guaiacol performed in the autoclave at 320 °C and initial hydrogen pressure of 17 MPa, reaction time – 1 h, m_{GUA}:m_{cat} = 33:1.

No.	Product	Ni30.3Cu10.4/CeO_2-ZrO_2 Yield (W_i) (%)	Ni14.1Cu5.7/Al_2O_3	Ni57.9Cu7.0/SiO_2	Ni36.5Cu2.3/ZrO_2-SiO_2-La_2O_3	Ni55.4/SiO_2
1	Cyclohexane	0.7	42.6	55.3	58.9	63.9
2	Benzene	0.2	0.8	4.9	9.8	16.4
3	1-Methylcyclohexane-1,2-diol	27.2	13.1	1.9	0.3	–
4	Cyclohexanone	58.1	12.5	3.9	1.4	0.6
5	Phenol	0.2	–	1.4	1.5	1.5
6	Methoxybenzene	0.2	0.3	1.1	0.5	0.6
7	Cyclopentanol	3.3	–	0.4	0.3	0.7
8	Cyclopentanone	3.1	–	0.2	0.1	–
9	Cyclohexene	–	1.1	0.5	0.4	–
10	Cyclohexanol	0.1	2.1	–	–	–
11	1,2-Cyclohexanediol	1.4	0.5	0.3	0.3	0.2
12	Methoxycyclohexane	–	–	0.1	–	–
13	1,2-Dimethoxycyclohexane	1.8	0.4	0.1	–	–
14	Methylguaiacols	–	0.7	0.6	–	0.1
15	Methylcyclohexane	–	1.5	1.1	0.7	1.1
16	Dimethylcyclopropane	0.7	5.3	6.4	9.3	5.0
17	Cyclopentane	–	1.3	5.0	5.4	6.5
18	Bicyclohexyl	–	0.4	2.4	0.7	2.0
19	2-Cyclohexylphenol	–	–	0.3	0.2	0.1
20	Cyclohexylbenzene	–	0.2	–	–	–
21	2-Cyclohexylcyclohexanol	–	0.5	1.1	0.7	0.3

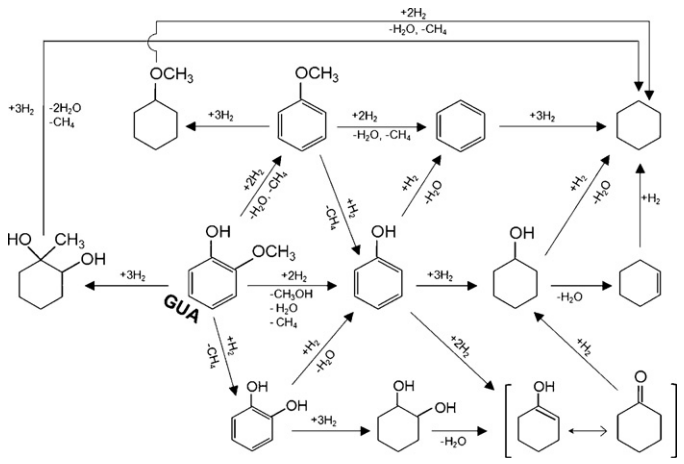

Scheme 1. Guaiacol conversion pathways over Ni-based catalysts.

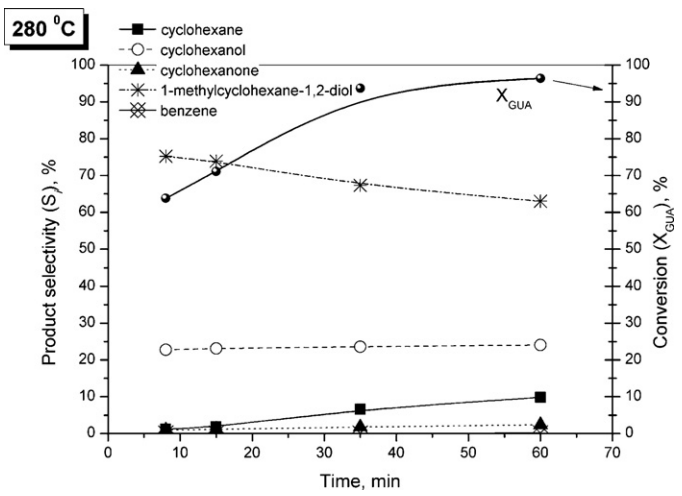

Fig. 3. Time dependence of guaiacol conversion and selectivity (S_i) towards main products of HDO of guaiacol over Ni36.5Cu2.3/ZrO_2-SiO_2-La_2O_3 at 280 °C, $\nu^0(H_2)/\nu^0(GUA)$ = 4.9 mol/mol.

substituted product (1-methyl-1,2-cyclohexandiol) was also observed in [14]. Nevertheless, no methylcatechols or any other methylated aromatic products were detected in the present study even in the case of Ni14.1Cu5.7/Al_2O_3 catalyst.

It should be noted that conversion schemes proposed in the previous studies of guaiacol and phenol HDO [11,19,37] included the direct transformation of catechol (in the case of guaiacol) and phenol (in both cases) into cyclohexanone. The mechanisms of such transformations were discussed in [20,38]. It was proposed that cyclohexanone might appear as an intermediate in the isomerization of the partial-hydrogenation product cyclohexenol (ketone/enol tautomerism). A thermodynamic assessment of cyclohexanol dehydrogenation into cyclohexanone revealed that this reaction is unlikely to occur, since the Gibbs energy change of this reaction is positive (ΔG = 68.5 kJ/mol at T = 320 °C). In the present work we also propose the mechanism of cyclohexanone formation through the keto-enol tautomerism, which is likely to perform with 1-cyclohexen-1-ol as an intermediate product.

3.2. Effect of temperature on HDO of guaiacol

Since Ni36.5Cu2.3/ZrO_2-SiO_2-La_2O_3 catalyst demonstrates the high activity in the target process of guaiacol HDO, this catalyst was used in the investigations of the temperature influence on the product distribution and the effectiveness of the overall process. Before the loading of guaiacol into the reactor, the catalyst (0.2 g, 0.05–0.1 mm fraction) was activated *in situ* with hydrogen, as described above. Three series of experiments were carried out at 280, 320, and 360 °C at different reaction times. All experiments were performed just once. A fresh catalyst was used at every run. Each time, the reactor was pressurized with pure hydrogen so that the pressure of 17 MPa was reached at the final temperature ($T_{reaction}$). Thus, the hydrogen-to-guaiacol molar ratio was the same within one series of experiments at a certain temperature.

Figs. 3–5 display the guaiacol conversion and the selectivity (S_i) towards the main products in dependence on time over Ni36.5Cu2.3/ZrO_2-SiO_2-La_2O_3 at 280, 320, and 360 °C. It is evident from Figs. 3–5 that the guaiacol conversion decreases with the increase in reaction temperature that is not typical of catalytic processes. On the other hand, it is known that oxygen-containing aromatic compounds with at least two functional groups are prone to polymerization. Therefore, the conversion decrease can be explained with the blocking of catalyst active centers by nascent high-molecular compounds [14,39]. The increasing temperature enhances the polymerization of oxy-organics. The polymerization products are precursors of coke, whose amount also increases with temperature [40,41].

The comparative analysis of the product distribution in guaiacol HDO at different temperatures showed the following tendencies:

- Oxygen-containing aliphatic compounds are formed primarily at low temperature (280 °C), whereas the increase in temperature leads to a significant increase in the selectivity towards cyclohexane as a final product in HDO of guaiacol.
- The selectivity to aromatic products (primarily benzene and phenol) increases with the temperature, which is in good agreement with [14].
- At high temperatures the products of the aromatic ring condensation and their subsequent hydrogenation (Fig. 2) are observed, which is in agreement with [11,14].

To prevent the repolymerization of biomass fast pyrolysis products and therefore the fast coking of the catalyst surface, the approach proposed by Venderbosch et al. [42] can be applied. This approach provides a two-stage HDO of bio-oil: hydrogenation and partial deoxygenation of unsaturated oxygen-containing organics

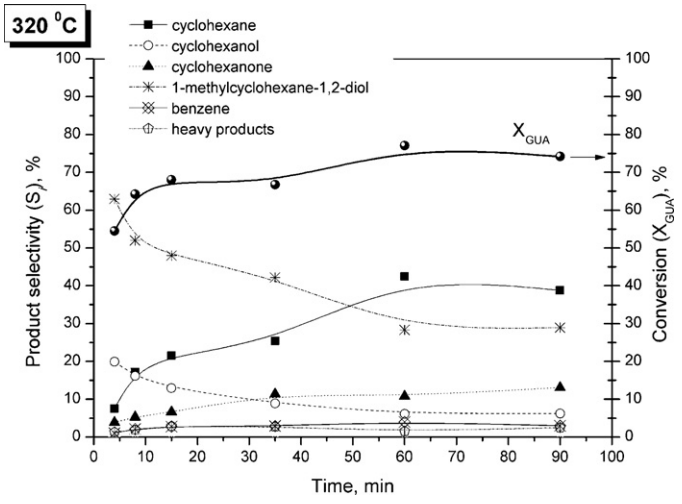

Fig. 4. Time dependence of guaiacol conversion and selectivity (S_i) towards main products of HDO of guaiacol over Ni36.5Cu2.3/ZrO_2-SiO_2-La_2O_3 at 320 °C, $\nu^0(H_2)/\nu^0(GUA)$ = 4.6 mol/mol.

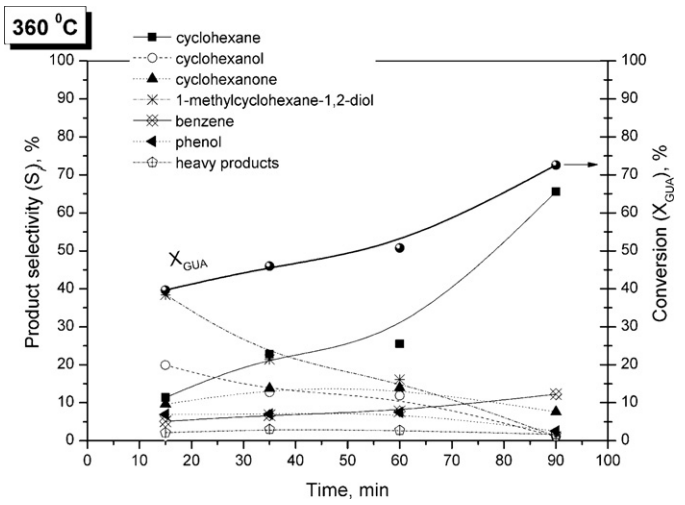

Fig. 5. Time dependence of guaiacol conversion and selectivity (S_i) towards main products of HDO of guaiacol over Ni36.5Cu2.3/ZrO_2-SiO_2-La_2O_3 at 360 °C, $\nu^0(H_2)/\nu^0(GUA)$ = 4.4 mol/mol.

at lower temperatures in the range 175–250 °C (1st stage) and a subsequent hydrotreatment at elevated temperatures in the range 350–400 °C (2nd stage).

According to the data presented in Fig. 6, the ratio $W_{Aliphatic}/W_{Aromatic}$ decreases with the temperature rise. Most likely, the contribution of guaiacol conversion stages (Scheme 1) based on the $C_{aromatic}$—O bond hydrogenolysis increases with temperature, which is in agreement with Ref. [14]. Fig. 6 also demonstrates the rise in the guaiacol deoxygenation degree with temperature. It indicates that the C—O bond hydrogenolysis starts to prevail over the aromatic ring hydrogenation with an increase in the reaction temperature.

3.3. Catalyst characterization by physicochemical methods

The Ni55.4/SiO_2, Ni57.9Cu7.0/SiO_2, and Ni36.5Cu2.3/ZrO_2-SiO_2-La_2O_3 catalysts, which showed the highest activities in HDO of guaiacol, were characterized by various physicochemical methods to find a correlation between the catalyst activity and catalyst structure. Comparing the catalyst textural characteristics (except for Ni36.5Cu2.3/ZrO2-SiO_2-La_2O_3) given in Table 1 with the guaiacol conversion and deoxygenation degree (Table 2), one can conclude that the catalyst activity correlates with the catalyst specific area. The Ni36.5Cu2.3/ZrO_2-SiO_2-La_2O_3 catalyst did not comply with this correlation due to the specificity of its preparation, when zirconia was added to the catalyst composition after the co-precipitation stage. ZrO_2 appeared as a binder required for the improvement of the catalyst mechanical and thermal stability. Besides, the preparation of this catalyst involved an impregnation with a promoting agent La_2O_3 used to improve the thermal stability of ZrO_2-containing catalysts [43].

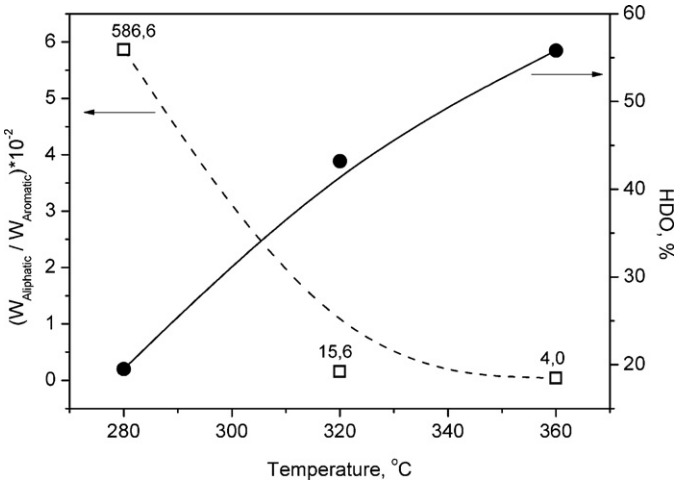

Fig. 6. Effect of temperature on the ratio of aliphatic to aromatic product yields ($W_{Aliphatic}/W_{Aromatic}$) (⋙) and the deoxygenation degree (•) in HDO of guaiacol. Reaction time of 35 min, P ($T_{reaction}$) = 17 MPa.

3.3.1. TPR study

All catalysts were characterized by the temperature-programmed reduction technique (Fig. 7) to determine the optimal temperature of catalyst preliminary reduction. The TPR profiles for the Ni55.4/SiO_2, Ni57.9Cu7.0/SiO_2, and Ni36.5Cu2.3/ZrO_2-SiO_2-La_2O_3 catalysts (Fig. 7a–c) prepared by the co-precipitation reveal a low-temperature peak centered at 170 °C. This peak can be ascribed to the reduction of Ni (III) species formed by oxygen chemisorption on highly dispersed NiO [44]. According to [44], the TPR profile of well-crystallized bulk NiO shows a single sharp peak with the maximum at 400 °C. A broad reduction peak, which is observed on the TPR profiles (Fig. 7a–c) between 300 and 700 °C, most likely indicates the strong interaction of components in these catalysts as a result of the formation of hardly reducible nickel silicates [31]. These samples apparently differ from the silicate-free catalysts prepared by the impregnation method (Fig. 7d–e). A small peak at 240 °C (Fig. 7a) corresponds to the reduction of weakly bound NiO, whose defective structure facilitates the reduction at lower temperatures as compared to well-crystallized bulk NiO.

Note that the TPR profiles of Cu-containing catalysts (Fig. 7b–e) reveal reduction peaks between 230 and 300 °C with the areas that correlate with the copper content. Thus, the intense reduction of these catalysts starts at lower temperature as compared with bulk NiO [44] and monometallic Ni55.4/SiO_2 (Fig. 7a). It is well known that copper oxides are reduced at 230–300 °C. Besides, the reduction temperature of nickel oxides is known to decrease in the presence of copper [45]. It was shown previously [10] that the reduction of nickel and copper mixed oxides results in the formation of Ni_xCu_{1-x} solid solutions. The formation of a Ni_xCu_{1-x} solid solution in our experiments is confirmed by an XRD analysis (see below). The reduction peaks at 240, 320, and 494 °C on the TPR profile of Ni14.1Cu5.7/Al_2O_3 (Fig. 7d) were attributed to (i) the low-temperature reduction of Ni(II) in the presence of copper, (ii) the reduction of NiO weakly bound to Al_2O_3, and (iii) the high-temperature reduction of a Ni(II) solid solution in Al_2O_3, respectively.

3.3.2. XRD study

The results of *in situ* X-ray diffraction investigation of Ni57.9Cu7.0/SiO_2 carried out in pure H_2 are presented in Fig. 8. The XRD pattern of a fresh Ni57.9Cu7.0/SiO_2 (Fig. 8a, Ox) shows broad peaks referred to the NiO phase with the slight shift of peaks relative to the reference data [46]. At that, the relative intensities of NiO lines do not match the reference data for the NiO crystalline phase, and the peaks are differently broadened.

There are different explanations of this phenomenon. First, it is the anisotropic form of NiO crystallites. Second, the CuO reflections on the XRD pattern of the fresh catalyst (Fig. 8a, Ox) probably overlap the 1 1 1 (2θ of 36°) and 220 (2θ of 62°) reflections from NiO and contribute to the NiO peak intensities. Besides, mixed SiO_2-NiO species with a silicate-like structure can contribute to these peaks as well. Similar X-ray diffraction patterns were observed for Ni55.4/SiO_2 and Ni36.5Cu2.3/ZrO_2-SiO_2-La_2O_3 catalysts obtained by the co-precipitation, which were also highly active in HDO of guaiacol [47].

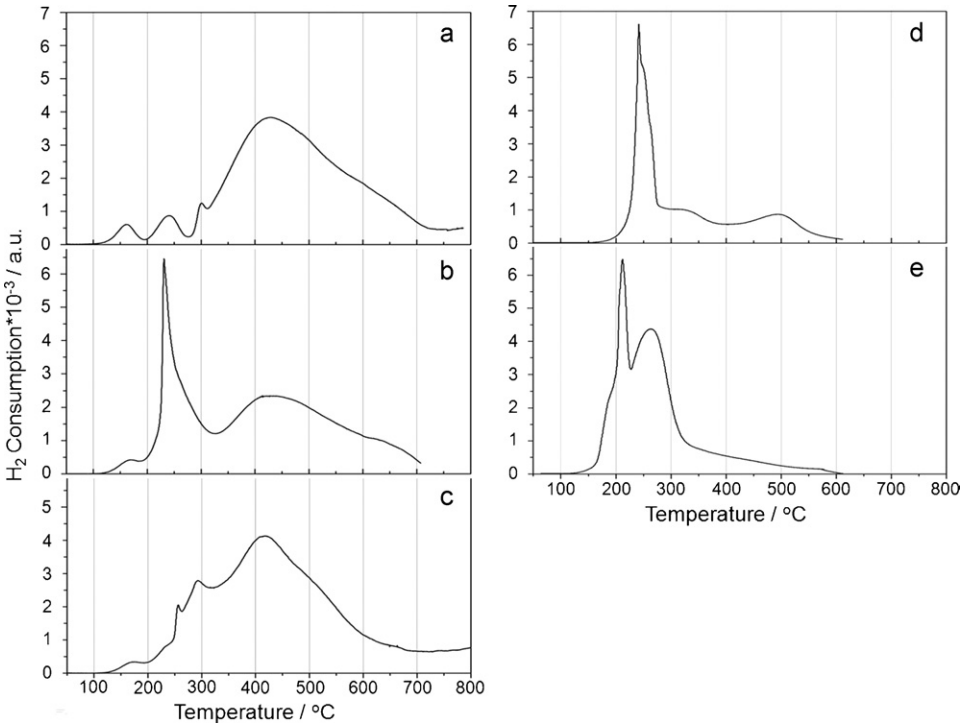

Fig. 7. TPR profiles of (a) Ni55.4/SiO_2, (b) Ni57.9Cu7.0/SiO_2, (c) Ni36.5Cu2.3/ZrO_2-SiO_2-La_2O_3, (d) Ni14.1Cu5.7/Al_2O_3, (e) Ni30.3Cu10.4/CeO_2-ZrO_2.

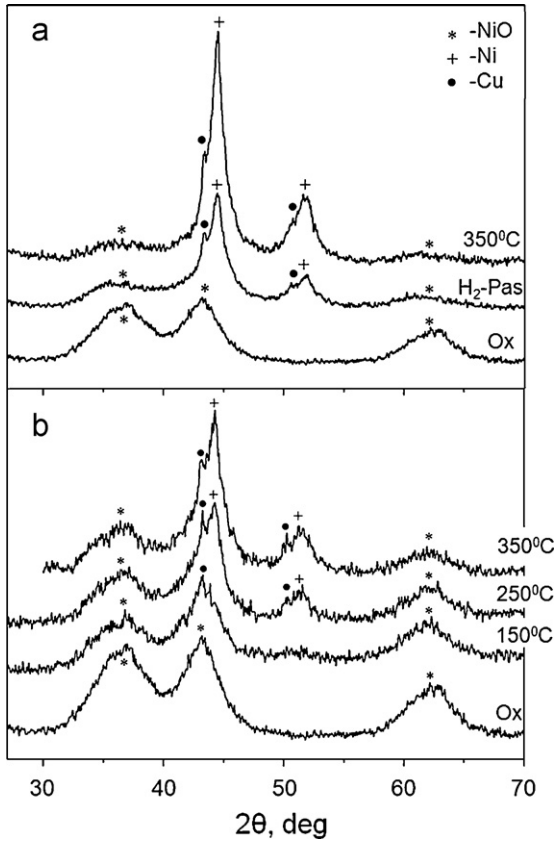

Fig. 8. XRD patterns of Ni57.9Cu7.0/SiO_2: (a) Ox – the fresh catalyst (oxide form); H_2-Pas – the sample reduced in the autoclave in pure H_2 at 400 °C and passivated with ethanol; 350 °C – the sample H_2-Pas after the subsequent reduction *in situ* in the diffractometer at 350 °C; (b) the fresh catalyst (Ox) after reducing *in situ* in the diffractometer at 150, 250, and 350 °C, correspondingly.

The XRD pattern of Ni57.9Cu7.0/SiO_2 reduced in the autoclave at 400 °C and passivated with ethanol (Fig. 8a, H_2-Pas) is somewhat different from the pattern of the fresh catalyst. The relative intensity of NiO peaks is observed to decrease. Besides, there appear the intense reflexes corresponding to nickel and copper in the metallic state. The diffraction pattern of this sample after the subsequent *in situ* reduction at 350 °C in pure H_2 (Fig. 8a, 350 °C) reveals the increase in the peak intensities corresponding to metallic Ni and Cu. This indicates the incomplete reduction of the catalyst during the preliminary treatment in H_2 at 400 °C. Note also that the Ni57.9Cu7.0/SiO_2 catalyst even after the prereduction in the autoclave at 400 °C and subsequent *in situ* reduction at 350 °C still retained nickel in the oxide form. These results correlate with the TPR data of Ni57.9Cu7.0/SiO_2, indicating that the catalyst reduction proceeds up to 700 °C.

The reflexes of the Ni metallic phase are narrowing during the reduction *in situ* (Fig. 8a, H_2-Pas and 350 °C) and the CSD of metallic nickel particles rises from 50 to 65 Å. This effect can be attributed to the agglomeration of metal particles on the surface of catalysts with the high metal loading. However, the accuracy of metallic Ni crystal size determination is not high due to the presence of the NiO line at 40–47°. The observed slight shift of the metallic nickel reflexes towards smaller 2θ angles as compared with the reference data [48] points to the formation of a Ni_xCu_y solid solution.

The reduction of Ni57.9Cu7.0/SiO_2 was also investigated *in situ*. In this experiment, the fresh catalyst was reduced in H_2 at preset temperatures (150, 250, and 350 °C), and corresponding *in situ* XRD patterns were obtained after cooling to room temperature in the reductive medium. These patterns are presented in Fig. 8b. The XRD pattern of the sample heated to 150 °C shows low intense reflexes attributed to metallic copper. This indicates the beginning of the catalyst reduction. Upon heating to higher temperatures, the relative intensity of peaks corresponding to NiO is observed to decrease. The intensity of metallic copper lines almost does not change, whereas the intensity of Ni reflexes continues to increase. These results indicate that copper oxide is reduced at lower

temperatures as compared to nickel oxide. Besides, the NiO reduction temperature decreases in the presence of copper, which is in agreement with the TPR data. The NiO peaks still remain on the catalyst XRD pattern after the *in situ* treatment in hydrogen at 350 °C, indicating incomplete catalyst reduction under these conditions. These observations, as well as shapes and positions of NiO peaks on the XRD pattern of the fresh Ni57.9Cu7.0/SiO_2 catalyst, suggest the formation of silicate-like species in the catalyst structure.

3.3.3. XPS study

The XPS analysis was carried out with three series of the catalysts: Ni55.4/SiO_2, Ni57.9Cu7.0/SiO_2, and Ni36.5Cu2.3/ZrO_2-SiO_2-La_2O_3. The samples were treated under the same conditions as for XRD analysis. Each series included three samples of one catalyst: No. 1 – the initial oxide sample (Ox) after calcination; No. 2 – the sample (H_2-Pas) after the reduction in the autoclave at 0.1 MPa H_2 at 400 °C and subsequent passivation with ethanol; No. 3 – sample No. 2 additionally reduced inside the high-pressure cell of the XPS spectrometer at 0.1 MPa H_2 at 400 °C.

Fig. 9 presents the Ni2p and Cu2$p_{3/2}$ core-level spectra of Ni57.9Cu7.0/SiO_2. Initial sample 1 (Ox) contains mainly nickel in the Ni^{2+}oxide state (Fig. 9a, Ni2p). It is indicated by the complex structure of the Ni2p spectrum, which reveals two sharp peaks corresponding to the Ni2$p_{3/2}$ and Ni2$p_{1/2}$ main lines at 855.9 and 873.5 eV, as well as intense shake-up satellites at 861.7 and 879.4 eV, respectively. The presence of shake-up satellites ascribed to a multiple electron excitation is typical of Ni^{2+} species. For example, the intense shake-up satellites are observed in the XPS spectra of NiO, $Ni(OH)_2$, $NiSiO_3$, *etc.* [49–56]. In contrast, spectra of metallic nickel and Ni^{3+} species do not show such satellites [56]. According to the reference data, the Ni2$p_{3/2}$ binding energy of NiO, $Ni(OH)_2$ and nickel silicates ($NiSiO_3$ and Ni_2SiO_4) lie in the ranges of 853.8–854.6, 855.5–855.9, and 856.3–856.7 eV, respectively [49–56]. Based on comparison of the Ni2$p_{3/2}$ binding energy (855.9 eV) of Ni57.9Cu7.0/SiO_2 with the reference data, we assumed that the nickel cations on the surface of catalyst 1 (Ox) are a part of nickel silicates or nickel hydroxides, but not NiO. Indeed, the Ni2$p_{3/2}$ peak at 855.9 eV has a symmetrical shape, whereas the Ni2p spectrum of bulk NiO shows an additional intense shake-up satellite shifted by 1.8–1.9 eV towards higher binding energies [49,53,54].

Sample 1 (Ox) contains copper mainly in the Cu^{2+} state. The Cu2p core-level spectrum, in addition to the main Cu2$p_{3/2}$ line at 934.0 eV, shows the intense shake-up satellite at 942.0 eV (Fig. 9a, Cu2$p_{3/2}$). This satellite is typical of the Cu^{2+} species and reflects the hybridization of Cu3d and O2p orbitals [49,57–63]. The spectra of Cu^{1+} species and of metallic copper do not reveal shake-up satellites. Moreover, the Cu2$p_{3/2}$ binding energies of metallic copper and Cu_2O are in the range of 932.4–932.9 eV, whereas the Cu2$p_{3/2}$ binding energy of CuO is in the range of 933.6–934.6 eV [49,57–63].

According to the reference data [50–52], the Si2p binding energy of silicates $NiSiO_3$ and Ni_2SiO_4 is in the range of 103.0–103.5 eV. In our case, the Si2p XPS spectrum of sample 1 (Ox) of the catalyst Ni57.9Cu7.0/SiO_2 showed a single peak at 102.2 eV (spectra not shown here). This shift towards lower binding energies is most probably due to the presence of copper cations in the catalyst. A somewhat higher binding energy (103.7 eV) is generally observed for Si^{4+} in SiO_2 [64]. Thus, it might be concluded that at the stage of oxide catalyst preparation (sample 1 (Ox)), the mixture of silicates $NiSiO_3$, Ni_2SiO_4 and/or nickel phyllosilicate $Si_2Ni_3O_5(OH)_4$ doped with Cu^{2+} is likely to form.

The Ni2p core-level spectrum of the reduced sample (sample 2 (H_2-Pas)) reveals two additional peaks at 852.7 and 869.9 eV (Fig. 9b, Ni2p), which undoubtedly correspond to nickel in the metallic state. Fig. 9 presents the Ni2p spectrum of a clean Ni foil (Fig. 9d, Ni2p) for comparison. Two sharp peaks at 852.7 and 869.9 eV correspond to the Ni2$p_{3/2}$—Ni2$p_{1/2}$ doublet, while the additional peaks at about 858.6 and 874.7 eV are due to the plasmon exitation [53]. To estimate the fraction of nickel in the metallic state, the spectrum was deconvoluted onto individual components. Correspondingly, only 15% of nickel in sample 2 (H_2-Pas) is in the metallic state (Table 4).

Table 4
Relative atomic concentrations (atomic ratios) of elements in the catalyst surface layer.

Sample	[Ni]/[Si]	[Ni^{2+}]:[Ni^0]	[Cu]/[Si]	[Cu]/[Ni]
Ni55.4/SiO_2				
No. 1 – Ox	0.83	100:0	–	–
No. 2 – H_2-Pas	0.51	73:27	–	–
No. 3 – H_2 *in situ*	0.18	0:100	–	–
Ni57.9Cu7.0/SiO_2				
No. 1 – Ox	1.70	100:0	0.14	0.08
No. 2 – H_2-Pas	0.81	85:15	0.03	0.04
No. 3 – H_2 *in situ*	0.29	0:100	0.06	0.19
Ni36.5Cu2.3/SiO_2-ZrO_2-La_2O_3				
No. 1 – Ox	3.00	100:0	0.18	0.06
No. 2 – H_2-Pas	1.10	66:34	0.06	0.05
No. 3 – H_2 *in situ*	0.32	0:100	0.06	0.19

After the additional treatment of sample 2 (H_2-Pas) in pure H_2 inside the XPS spectrometer (sample 3), the Ni2p spectrum (Fig. 9c, Ni2p) became almost identical to that of a clean Ni foil (Fig. 9d, Ni2p), indicating the complete reduction of Ni^{2+} species in the catalyst surface layer. The analysis depth of XPS is about 3–6 nm. The nickel reduction is accompanied by a decrease in the [Ni]/[Si] atomic ratio that points to the formation of large metal particles on the catalyst surface (Table 4). Indeed, the atomic ratio [Ni]/[Si] is 1.7 for sample 1 (Ox), and 0.81 for reduced sample 2 (H_2-Pas). After the reduction inside the XPS spectrometer (sample 3) the atomic ratio [Ni]/[Si] decreases to 0.29.

Copper is almost completely reduced in sample 2 (H_2-Pas). The Cu2$p_{3/2}$ core-level spectrum reveals a symmetric narrow peak at 932.6 eV (Fig. 9b, Cu2$p_{3/2}$). For catalyst 3, the Cu2$p_{3/2}$ binding energy is 932.4 eV (Fig. 9c, Cu2$p_{3/2}$). Unfortunately, the Cu2$p_{3/2}$ binding energy of Cu^0 and Cu^{1+} species is almost the same, which hampers its identification [49,57–61]. The Auger-parameter α, which is equal to the sum of the Cu2$p_{3/2}$ binding energy and of the CuLMM kinetic energy [65], can be used for this goal. According to the reference data [59–63], the Auger-parameters of metallic Cu, Cu_2O, and CuO lie in the ranges of 1851.0–1851.4, 1848.7–1849.3, and 1851.4–1851.7 eV, respectively. The Auger-parameter of the catalyst reduced inside the XPS spectrometer (sample 3) is 1850.8 eV, which is typical of metallic copper (Fig. 9c, Cu2$p_{3/2}$). A small difference from the reference data can be due to the high dispersion of copper particles or the formation of a NiCu solid solution. The atomic ratio [Cu]/[Si] decreases from 0.14 for the initial oxide sample (sample 1(Ox)) to 0.03 for sample 2 (H_2-Pas) (Table 4). In the case of sample 3, the atomic ratio [Cu]/[Si] increases up to 0.06. By analogy, the atomic ratio [Cu]/[Ni] decreases from 0.08 for sample 1 (Ox) to 0.04 for sample 2 (H_2-Pas), and after the additional reduction inside the XPS spectrometer (sample 3) it reaches the value of 0.19. Therefore, the copper segregation can be assumed to occur on the surface of nickel particles during the reduction.

Similar results were obtained for the other two series of the catalysts: Ni55.4/SiO_2 and Ni36.5Cu2.3/ZrO_2-SiO_2-La_2O_3. In the case of Ni55.4/SiO_2, the Ni2p XPS spectra are the same as depicted in Fig. 9 for the Ni57.9Cu7.0/SiO_2 catalyst. The Si2p core-level spectrum shows a single peak at 103.0 eV that is typical of Si^{4+} species in the silicate structure. In the case of Ni36.5Cu2.3/ZrO_2-SiO_2-La_2O_3, the Ni2p and Cu2$p_{3/2}$ core-level spectra also coincide with those

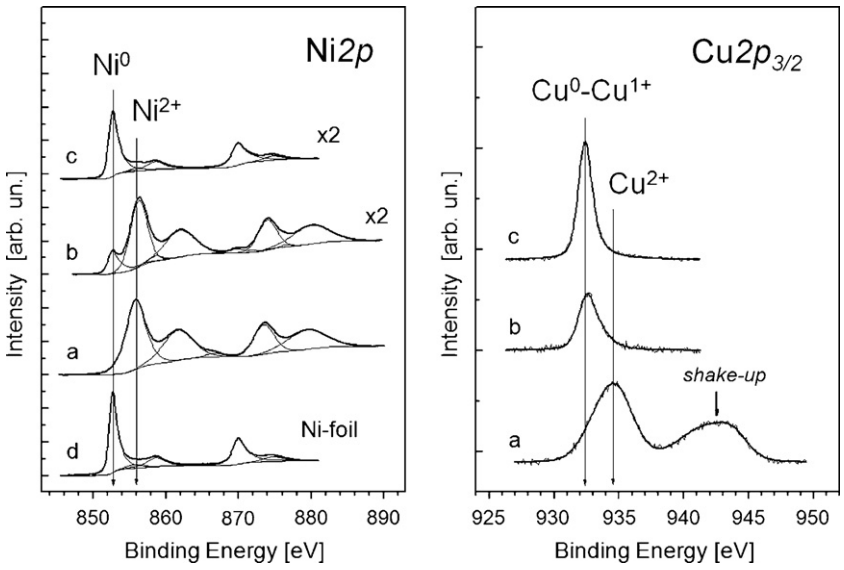

Fig. 9. The Ni2p and $Cu2p_{3/2}$ core-level spectra of a series of the $Ni57.9Cu7.0/SiO_2$ catalyst: (a) – sample 1 (Ox) (initial oxide form), (b) – sample 2 (H_2-Pas) (after the reduction of sample 1 (Ox) in 0.1 MPa H_2 at 400 °C and subsequent passivation with ethanol), (c) – sample 3 obtained by the additional reduction of catalyst 2 inside the XPS spectrometer (400 °C, 0.1 MPa H_2). The spectra were normalized to the integral intensity of corresponding Si2p spectra. The Ni2p spectrum of a clean nickel foil (d) is displayed for comparison.

presented in Fig. 9, while the Si2p spectrum shows a single peak at 102.2 eV.

Fig. 10 displays the Zr3d core-level spectra of the series of the $Ni36.5Cu2.3/ZrO_2$-SiO_2-La_2O_3 catalyst. The Zr3d spectrum represents a doublet $Zr3d_{5/2}$—$Zr3d_{3/2}$, where the peak integral intensities relate as 3:2 and the spin–orbit splitting is 2.43 eV. The $Zr3d_{5/2}$ binding energy of sample 1 (Ox) is 182.0 eV (Fig. 10a), which is typical of Zr^{4+} species in the ZrO_2 structure. Indeed, the $Zr3d_{5/2}$ binding energy of the stoichiometric oxide ZrO_2 lies in the range 181.9–183.3 eV, whereas the binding energies of zirconium silicate $ZrSiO_4$ and mesoporous silicates doped with zirconium are somewhat higher (183.0–183.3 eV and 183.1–183.6 eV, respectively) [66,67]. The $Zr3d_{5/2}$ binding energies of the sample 2 (H_2-Pas) (Fig. 10b) and sample 3 (Fig. 10c) are 182.5 and 182.8 eV, respectively. This indicates that in the case of $Ni36.5Cu2.3/ZrO_2$-SiO_2-La_2O_3 (sample 1), zirconium is a part of only ZrO_2 and no Si–Zr mixed compounds are formed due to the catalyst preparation method used. The shift towards higher binding energies observed for the reduced samples can be ascribed to the formation of complex zirconium-based oxides during the catalyst treatment in hydrogen (Fig. 10b–c). The formation of nickel and copper zirconates also cannot be excluded.

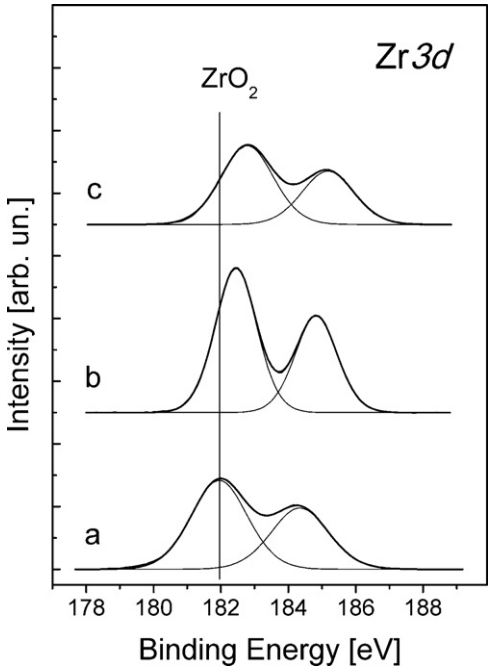

Fig. 10. The Zr3d core-level spectra of a series of the $Ni36.5Cu2.3/ZrO_2$-SiO_2-La_2O_3 catalyst: (a) – sample 1 (Ox) (initial oxide form), (b) –sample 2 (H_2-Pas) (after the reduction of sample 1 (Ox) in 0.1 MPa H_2 at 400 °C and subsequent passivation with ethanol), (c) – sample 3 obtained by the additional reduction of catalyst 2 inside the XPS spectrometer (400 °C, 0.1 MPa H_2).

3.3.4. HRTEM study

The HRTEM images of $Ni57.9Cu7.0/SiO_2$ reduced at 400 °C in the autoclave at 0.1 MPa H_2 and subsequently passivated with ethanol (H_2-Pas) are presented in Fig. 11. In good agreement with the XPS and XRD results, these images clearly demonstrate well-defined particles of metallic nickel, which are uniformly distributed throughout the catalyst. One can also see that the catalysts possess a lamellar structure formed by the thin flakes (1–2 nm) probably consisted of oxide–silicates. This is in agreement with the XRD data, according to which the XRD pattern of the initial catalyst reveals differently broadened NiO reflections corresponding to different crystallographic directions. The same morphology is characteristic of the $Ni55.4/SiO_2$ catalyst as well. The lamellar structure is also observed for the catalyst $Ni36.5Cu2.3/ZrO_2$-SiO_2-La_2O_3 (not presented in Fig. 11), however, it is mainly covered by bulk ZrO_2 particles due to the high content of ZrO_2 in the catalyst.

Hence, based on the presented results, it can be concluded that in the initial oxide form of the catalysts, nickel is a constituent of mainly silicate-like compounds with the lamellar structure (flake thickness of 1–2 nm). Most likely, namely this lamellar structure provides the high specific surface area of the active component (Ni) in these catalysts and hence their higher activity as compared to the catalysts obtained by impregnation. The XPS analysis showed that during the reduction at 400 °C nickel in the oxide–silicate structures was completely reduced in the surface layer of at least 6 nm thick with the partial agglomeration of nickel particles. On the other hand, the XRD analysis showed that nickel partly remains in the

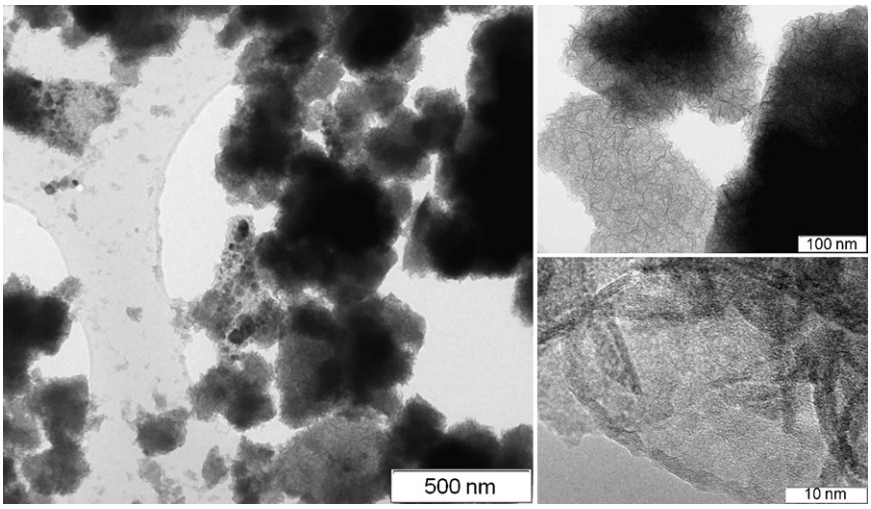

Fig. 11. HRTEM images of Ni57.9Cu7.0/SiO_2 reduced by hydrogen (0.1 MPa) at 400 °C (sample 2 (H_2-Pas)).

oxide state even after all stages of the reduction. This indicates that the oxide–silicate nickel phase is preserved in the bulk of the catalyst particle. The presence of copper is shown to promote the reduction of nickel oxide species at lower temperatures as compared to bulk NiO and Ni55.4/SiO_2. This effect was observed even for Ni-Cu catalysts with the hardly reducible nickel–silicate structure. Besides, the addition of copper diminishes the coke formation on the nickel phase and therefore reduces the catalyst deactivation. Hereafter, the improvement of the active component stability would require the addition of different modifying agents that can prevent the agglomeration of active metal particles.

4. Conclusions

The performance of Ni-based catalysts obtained by the co-precipitation and impregnation techniques has been investigated in the hydrodeoxygenation of guaiacol. The catalysts obtained by co-precipitation were notable for the high content of active component (Ni, 37–58 wt%) stabilized by SiO_2 and/or ZrO_2. Copper was applied as a promoter primarily to decrease the reduction temperature of nickel oxide forms. Catalyst testing in the autoclave at 320 °C and initial hydrogen pressure of 17 MPa revealed that the main products of guaiacol conversion (cyclohexane, cyclohexanone and 1-methylcyclohexane-1,2-diol) were formed by the partial or total deoxygenation and hydrogenation of the aromatic ring. Based on the experimental results, the guaiacol conversion scheme has been proposed to include products of the aromatic ring hydrogenation (such as 1,2-cyclohexanediol, 1-methylcyclohexane-1,2-diol), hydrodeoxygenation products (methoxybenzene, benzene, phenol), and products of hydrogenation and hydrodeoxygenation (cyclohexane, cyclohexanone, cyclohexene, cyclohexanol, methoxycyclohexane). Cyclohexanone was supposed to originate from unstable 1-cyclohexen-1-ol through keto-enol tautomerism.

Taking into account such reaction parameters as guaiacol conversion, deoxygenation degree, the amount of undesired gaseous products, and coke deposition, the catalyst Ni36.5Cu2.3/ZrO_2-SiO_2-La_2O_3 was chosen as the most promising catalytic system.

The effect of temperature (280, 320, and 360 °C) on the product distribution has been investigated over Ni36.5Cu2.3/ZrO_2-SiO_2-La_2O_3. The following regularities have been revealed: the deoxygenation degree increases with temperature, whereas the guaiacol conversion, on the contrary, decreases due to catalyst coking at elevated temperatures. To prevent intense coking of the catalyst, a special approach should be applied. This approach consists in the two-stage bio-oil hydrodeoxygenation: hydrogenation and partial deoxygenation of unsaturated oxygen-containing organics at a lower temperature in the range 175–250 °C (1st stage) and the hydrotreatment at elevated temperature in the range 350–400 °C (2nd stage). It was also shown that the C—O bond hydrogenolysis starts to prevail over aromatic ring hydrogenation with the temperature rise.

According to XRD, XPS, and HRTEM, the high activity of sol–gel Ni55.4/SiO_2, Ni57.9Cu7.0/SiO_2, Ni36.5Cu2.3/ZrO_2-SiO_2-La_2O_3 catalysts in HDO of guaiacol is determined by the high specific surface area of the active component (Ni) due to the formation of nickel oxide–silicate species in the form of thin layered flakes with a thickness of 1–2 nm. During the catalyst reduction under reaction conditions, the surface nickel oxide–silicate species undergo the total reduction, resulting in the partial agglomeration of active metal particles. However, the bulk oxide–silicate phase of the catalyst is not reduced, preserving the catalyst morphology. The addition of copper decreases the reduction temperature of the nickel oxide forms and prevents excessive carbon deposition on the nickel phase, therefore reducing the catalysts deactivation rate.

In general, Ni-based catalysts for hydrodeoxygenation of real bio-oil should meet the following requirements.

- Nickel oxide species on the catalyst surface are to be reduced under the reaction conditions. Since hydrodeoxygenation proceeds by the redox mechanism, the special conditions are required for the reverse reduction of the surface oxide nickel species.
- Since bio-oil contains up to ~25 wt% of water and is characterized by pH ~2–3, the catalysts for HDO of bio-oil must be stable against the adverse effect of the acidic medium during the hydrothermal treatment.
- To improve the thermal stability of the catalysts, the catalyst active component has to be stabilized by the use of stabilizing agents and/or by some special approaches to the catalyst synthesis. Taking into account the specificity of bio-oil, one can expect a quick deactivation due to coke formation for catalysts of any type. High thermal stability of the catalysts in HDO of bio-oil is necessary for catalyst multiple regeneration without a loss of activity.

If the requirements established for the Ni-based catalysts of bio-oil HDO are satisfied, the intense development of such bioenergetics sectors as the production of liquid hydrocarbon fuel from wood, edible and non-edible oil crops and microalgae lipids is to be expected [68].

Acknowledgments

The work was performed under state contract No. 16.526.11.6003 and state contract No. 16.516.11.6049.

References

[1] A.V. Bridgwater, Biomass Bioenergy, doi:10.1016/j.biombioe.2011.01.048.
[2] T. Sfetsas, C. Michailof, A. Lappas, Q. Li, B. Kneale, J. Chromatogr. A 1218 (2011) 3317–3325.
[3] A. Oasmaa, E. Kuoppala, A. Ardiyanti, R.H. Venderbosch, H.J. Heeres, Energy Fuels 24 (2010) 5264–5272.
[4] Q. Lu, W.-Z. Li, X.-F. Zhu, Energy Convers. Manag. 50 (2009) 1376–1383.
[5] P.M. Mortensen, J.-D. Grunwaldt, P.A. Jensen, K.G. Knudsen, A.D. Jensen, Appl. Catal. A 407 (2011) 1–19.
[6] T.V. Choudhary, C.B. Phillips, Appl. Catal. A 397 (2011) 1–12.
[7] W.-Y. Wang, Y.-Q. Yang, H. Luo, T. Hu, W.-Y. Liu, Catal. Commun. 12 (2011) 436–440.
[8] Y. Yang, A. Gilbert, C. Xu, Appl. Catal. A 360 (2009) 242–249.
[9] A.R. Ardiyanti, A. Gutierrez, M.L. Honkela, A.O.I. Krause, H.J. Heeres, Appl. Catal. A 407 (2011) 56–66.
[10] V.A. Yakovlev, S.A. Khromova, O.V. Sherstyuk, V.O. Dundich, D.Y. Ermakov, V.M. Novopashina, M.Y. Lebedev, O. Bulavchenko, V.N. Parmon, Catal. Today 144 (2009) 362–366.
[11] V.N. Bui, G. Toussaint, D. Laurenti, C. Mirodatos, C. Geantet, Catal. Today 143 (2009) 172–178.
[12] J. Wildschut, I. Melián-Cabrera, H.J. Heeres, Appl. Catal. B 99 (2010) 298–306.
[13] A. Oasmaa, E. Kuoppala, Energy Fuels 22 (2008) 4245–4248.
[14] A. Gutierrez, R.K. Kaila, M.L. Honkela, R. Slioor, A.O.I. Krause, Catal. Today 147 (2009) 239–246.
[15] H.Y. Zhao, D. Li, P. Bui, S.T. Oyama, Appl. Catal. A 391 (2011) 305–310.
[16] Y.-C. Lin, C.-L. Li, H.-P. Wan, H.-T. Lee, C.-F. Liu, Energy Fuels 25 (2011) 890–896.
[17] T. Nimmanwudipong, R.C. Runnebaum, D.E. Block, B.C. Gates, Catal. Lett. 141 (2011) 779–783.
[18] C. Sepulveda, K. Leiva, R. Garcia, L.R. Radovic, I.T. Ghampson, W.J. DeSisto, J.L. Garcia Fierro, N. Escalona, Catal. Today 172 (2011) 232–239.
[19] V.N. Bui, D. Laurenti, P. Afanasiev, C. Geantet, Appl. Catal. B 101 (2011) 239–245.
[20] C. Zhao, J. He, A.A. Lemonidou, X. Li, J.A. Lercher, J. Catal. 280 (2011) 8–16.
[21] E. Furimsky, Appl. Catal. A 199 (2000) 147–190.
[22] Y. Xu, T. Wang, L. Ma, Q. Zhang, W. Liang, Appl. Energy 87 (2010) 2886–2891.
[23] N. Li, G.W. Huber, J. Catal. 270 (2010) 48–59.
[24] R. Nava, B. Pawelec, P. Castaño, M.C. Álvarez-Galván, C.V. Loricera, J.L.G. Fierro, Appl. Catal. B 92 (2009) 154–167.
[25] W.-Y. Wang, Y.-Q. Yang, J.-G. Bao, Z. Chen, J. Fuel Chem. Technol. 37 (2009) 701–706.
[26] S.T. Oyama, T. Gott, H. Zhao, Y.-K. Lee, Catal. Today 143 (2009) 94–107.
[27] P.G. Savva, K. Goundani, J. Vakros, K. Bourikas, C. Fountzoula, D. Vattis, A. Lycourghiotis, C. Kordulis, Appl. Catal. B 79 (2008) 199–207.
[28] L. De Rogatis, T. Montini, A. Cognigni, L. Olivi, P. Fornasiero, Catal. Today 145 (2009) 176–185.
[29] J.-H. Lee, E.-G. Lee, O.-S. Joo, K.-D. Jung, Appl. Catal. A 269 (2004) 1–6.
[30] RUS Patent 2335340 (2007).
[31] M.A. Ermakova, D.Y. Ermakov, Appl. Catal. A 245 (2003) 277–288.
[32] J.H. Scofield, J. Electron Spectrosc. Relat. Phenom. 8 (1976) 129–137.
[33] D.A. Shirley, Phys. Rev. B 5 (1972) 4709–4714.
[34] CasaXPS//www.casaxps.com.
[35] A. Centeno, E. Laurent, B. Delmon, J. Catal. 154 (1995) 288–298.
[36] V.O. Dundich, S.A. Khromova, D.Y. Ermakov, M.Y. Lebedev, V.M. Novopashina, V.G. Sister, A.I. Yakimchuk, V.A. Yakovlev, Kinet. Catal. 51 (2010) 704–709.
[37] W.-Y. Wang, Y.-Q. Yang, H. Luo, T. Hu, W.Y. Liu, React. Kinet. Mech. Catal. 102 (2011) 207–217.
[38] C. Zhao, Yu Kou, A.A. Lemonidou, Xu Li, J.A. Lercher, Angew. Chem. Int. Ed. 48 (2009) 3987–3990.
[39] F.P. Petrocelli, M.T. Klein, Fuel Sci. Technol. Int. 5 (1987) 25–62.
[40] R.K. Sharma, N.N. Bakhshi, Energy Fuels 7 (1993) 306–314.
[41] J.D. Adjaye, N.N. Bakhshi, Fuel Process. Technol. 45 (1995) 185–202.
[42] R.H. Venderbosch, A.R. Ardiyanti, J. Wildschut, A. Oasmaa, H.J. Heeres, J. Chem. Technol. Biotechnol. 85 (2010) 674–686.
[43] P.D.L. Mercera, J.G. van Ommen, E.B.M. Doesburg, A.J. Burggraaf, J.R.H. Ross, Appl. Catal. 71 (1991) 363–391.
[44] B. Mile, D. Stirling, M.A. Zammitt, A. Lovell, M. Webb, J. Catal. 114 (1988) 217–229.
[45] A. Crucq, L. Degols, G. Lienard, A. Frennet, Stud. Surf. Sci. Catal. 17 (1983) 137–147.
[46] PDF. # 471049.
[47] M.V. Bykova, O.A. Bulavchenko, D.Y. Ermakov, M.Y. Lebedev, V.A. Yakovlev, V.N. Parmon, Catal. Ind. 3 (2011) 15–22.
[48] PDF. # 040850.
[49] N.S. McIntyre, M.G. Cook, Anal. Chem. 47 (1975) 2208–2213.
[50] R.B. Shalvoy, P.J. Reucroft, J. Catal. 56 (1979) 336–348.
[51] M.L. Occelli, D. Psaras, S.L. Suib, J.M. Stencel, Appl. Catal. 28 (1986) 143–160.
[52] P. Lorenz, J. Finster, G. Wendt, J.V. Salyn, E.K. Zumadilov, V.I. Nefedov, J. Electron Spectrosc. Relat. Phenom. 16 (1979) 267–276.
[53] C.P. Li, A. Proctor, D.M. Hercules, Appl. Spectrosc. 38 (1984) 880–886.
[54] C.E. Dube, B. Workie, S.P. Kounaves, A. Rabbat, M.L. Aksu Jr., G. Davies, J. Electrochem. Soc. 142 (1995) 3357–3365.
[55] N.V. Kosova, E.T. Devyatkina, V.V. Kaichev, J. Power Sources 174 (2007) 735–740.
[56] A.F. Carley, S.D. Jackson, J.N. O'Shea, M.W. Roberts, Surf. Sci. 440 (1999) L868–L874.
[57] J.C. Otamiri, S.L.T. Andersson, A. Andersson, Appl. Catal. 65 (1990) 159–174.
[58] A. Wöllner, F. Lange, H. Schmelz, H. Knözinger, Appl. Catal. A 94 (1993) 181–203.
[59] J. Batista, A. Pintar, D. Mandrino, M. Jenko, V. Martin, Appl. Catal. A 206 (2001) 113–124.
[60] B.R. Strohmeier, D.E. Leyden, R.S. Field, D.M. Hercules, J. Catal. 94 (1985) 514–530.
[61] M. Richter, M.J.G. Fait, R. Eckelt, M. Scneider, J. Radnik, D. Heidemann, R. Fricke, J. Catal. 245 (2007) 11–24.
[62] V.I. Bukhtiyarov, V.V. Kaichev, I.P. Prosvirin, Top. Catal. 32 (2005) 3–15.
[63] S. Poulston, P.M. Parlett, P. Stone, M. Bowker, Surf. Interface Anal. 24 (1996) 811–820.
[64] A.A. Khassin, T.M. Yurieva, M.P. Demeshkina, G.N. Kustova, I.S. Itenberg, V.V. Kaichev, L.M. Plyasova, V.F. Anufrienko, I.Y. Molina, T.V. Larina, N.A. Baronskaya, V.N. Parmon, Phys. Chem. Chem. Phys. 5 (2003) 4025–4031.
[65] G. Moretti, J. Electron Spectrosc. Relat. Phenom. 76 (1995) 365–370.
[66] D.J. Jones, J. Jimenez-Jimenez, A. Jimenez-Lopez, P. Maireles-Torres, P. Olivera-Pastor, E. Rodriguez-Castellon, J. Roziere, Chem. Commun. (1997) 431–432.
[67] M.J. Guittet, J.P. Crocombette, M. Gautier-Soyer, Phys. Rev. B 63 (2001) 125117.
[68] V.A. Yakovlev, S.A. Khromova, V.I. Bukhtiyarov, Russ. Chem. Rev 80 (2011) 911–925.